

See discussions, stats, and author profiles for this publication at: <https://www.researchgate.net/publication/262817136>

# Structural and Energetic Insight into the Cross-seeding Amyloid Assemblies of Human IAPP and Rat IAPP.

ARTICLE *in* THE JOURNAL OF PHYSICAL CHEMISTRY B · JUNE 2014

Impact Factor: 3.3 · DOI: 10.1021/jp5022246 · Source: PubMed

---

CITATIONS

4

---

READS

15

## 7 AUTHORS, INCLUDING:



Mingzhen Zhang

University of Akron

17 PUBLICATIONS 60 CITATIONS

[SEE PROFILE](#)



Yung Chang

Chung Yuan Christian University

137 PUBLICATIONS 2,932 CITATIONS

[SEE PROFILE](#)

# Structural and Energetic Insight into the Cross-Seeding Amyloid Assemblies of Human IAPP and Rat IAPP

Mingzhen Zhang,<sup>†,‡</sup> Rundong Hu,<sup>†,‡</sup> Guizhao Liang,<sup>‡</sup> Yung Chang,<sup>§</sup> Yan Sun,<sup>||,⊥</sup> Zhenmeng Peng,<sup>†</sup> and Jie Zheng\*,<sup>†,⊥</sup>

<sup>†</sup>Department of Chemical and Biomolecular Engineering, The University of Akron, Akron, Ohio 44325, United States

<sup>‡</sup>Key Laboratory of Biorheological Science and Technology, Ministry of Education, Bioengineering College, Chongqing University, Chongqing 400044, China

<sup>§</sup>R&D Center for Membrane Technology and Department of Chemical Engineering, Chung Yuan University, Chung Li, Taoyuan 320, Taiwan

<sup>||</sup>Department of Biochemical Engineering and Key Laboratory of Systems Bioengineering of the Ministry of Education, School of Chemical Engineering and Technology, Tianjin University, Tianjin 300072, China

<sup>⊥</sup>Collaborative Innovation Center of Chemical Science and Engineering (Tianjin), Tianjin 300072, China

**ABSTRACT:** The misfolding and aggregation of human islet amyloid polypeptide (hIAPP or amylin) into small oligomers and large amyloid fibrils is believed to be responsible for the dysfunction and death of pancreatic  $\beta$ -cells in diabetes type II. However, rat IAPP (rIAPP), which differs from the hIAPP by only 6 of 37 residues, lacks the ability to form amyloid fibrils and to induce cell death. Little is known about the cross-sequence interactions and cross-seeding structures between hIAPP and rIAPP peptides. Herein using explicit-solvent molecular dynamics (MD) simulations, we modeled and simulated different heteroassemblies formed by the amyloidogenic hIAPP and the nonamyloidogenic rIAPP peptides. Simulations showed that the U-shaped hIAPP monomer and oligomers can interact with conformationally similar rIAPP to form stable complexes and to coassemble into heterogeneous structures. Stable heterointeractions between hIAPP and rIAPP were shown to arise from hydrophobic contacts and hydrogen bonds at the interface, particularly at N- and C-terminal  $\beta$ -sheet regions. Because of the enhanced interpeptide interactions at the interface, upon binding to hIAPP oligomers, the  $\beta$ -sheet population of rIAPP was greatly increased as compared to that of rIAPP alone. More importantly, the conformational energies of rIAPP monomers at the bound state were observed to be consistently higher than those of rIAPP monomers at the unbound state. However, rIAPP monomers enable one to adopt different conformations and follow different pathways for associating with hIAPP from the high energy of the bound state to the low energy of the unbound state, without encountering any large and abrupt energy barrier. In parallel, AFM study of cross-aggregation of hIAPP and rIAPP provided additional evidence that hIAPP can seed with rIAPP to form hybrid fibrils at all concentrations similar to pure hIAPP fibrils. This work demonstrates the existence of cross-interactions between the two different IAPP peptides, which provides an improved fundamental understanding of the cross-seeding of different amyloid sequences toward amyloid aggregation and toxicity mechanisms.



## INTRODUCTION

Human islet amyloid polypeptide (hIAPP or amylin) is a causative molecule in pancreatic amyloid deposits found in the majority of patients with type-II diabetes (T2D). hIAPP, a 37-residue hormone peptide that is normally produced and cosecreted with insulin by pancreatic islet  $\beta$ -cells, achieves its multiple physiological functions by regulating glucose homeostasis, glucagons release, and gastric emptying.<sup>1</sup> Meanwhile, under the disease conditions, hIAPP can misfold and self-aggregate into small soluble oligomers and large insoluble amyloid fibrils, and some of them are pathologically associated with the dysfunction and death of islet  $\beta$ -cells, the production and action of insulin production, and the activation of calcitonin receptor in T2D.<sup>2</sup> While the precise mechanisms of amyloid formation and cytotoxicity of hIAPP are still not well

understood, increasing evidence has supported that amyloid cytotoxicity is very likely related to the formation of hIAPP oligomers, which are thought to be very toxic species to  $\beta$ -cells.<sup>3</sup> Several plausible models<sup>5,10–14</sup> have argued that interactions of hIAPP oligomers with cell membranes enable to disrupt the integrity, permeability, and functions of cell membranes, leading to ionic homeostasis, changes of signaling pathways, oxidative injury, and cell death ultimately.<sup>4–9</sup> Similar amyloid aggregation and toxicity behaviors were also observed by other amyloidogenic peptides including amyloid- $\beta$  ( $A\beta$ ) peptide linked to Alzheimer's disease<sup>10</sup> and  $\alpha$ -synuclein peptide

Received: March 4, 2014

Revised: May 28, 2014

Published: June 3, 2014

linked to Parkinson's disease.<sup>11</sup> Thus, inhibition of amyloid aggregation and formation is considered as one of the key therapeutic approaches against T2D and other amyloid diseases.

Rat IAPP (rIAPP) differs from hIAPP by only 6 of 37 residues, but rIAPP lacks the ability to form amyloid and is nontoxic to  $\beta$ -cells. Five of six different residues of rIAPP (H18R, F23L, A25P, I26V, S28P, and S29P) locate at a primary amyloidogenic region (positions 20–29). Early studies have shown that the 20–29 sequence plays a determinant role in amyloid formation by hIAPP. Moreover, rIAPP contains three proline residues at 25, 28, and 29 positions, which could contribute to the inability of rIAPP to form amyloid as well, in agreement with the general  $\beta$ -sheet blocker role of proline residues in other proteins. rIAPP lacks the ability to aggregate into  $\beta$ -sheet-rich species,<sup>12</sup> which has been implicated to its nontoxic nature to cells. Due to the high sequence similarity and nonamyloidogenic nature of rIAPP, not surprisingly, rIAPP has been used as the basis for design of inhibitors against hIAPP aggregation and toxicity. A number of experimental studies have shown that rIAPP and its analogues, such as A13P–rIAPP and F15D–rIAPP, inhibit amyloid formation by hIAPP, prolonging both lag and growth phases in a dose-dependent manner.<sup>13</sup> Recently, Middleton et al.<sup>14</sup> found a dual role of rIAPP in hIAPP amyloid formation when coincubating rIAPP with hIAPP. At the early stage of hIAPP aggregation, rIAPP initially prevented the  $\beta$ -sheet formation of hIAPP, as indicated by a prolonging of a lag phase. However, once hIAPP seeds or protofibrils were formed as time processed, hIAPP seeds could recruit rIAPP and grow them onto hIAPP seeds to promote the formation of hybrid amyloid fibrils eventually. The early studies seem to be controversial with conflicting data. The precise biological role of rIAPP as an inhibitor or a catalyst in preventing or promoting the amyloid formation of hIAPP is still not well understood, but some studies have shown that cross-seeding of different but conformationally similar peptides may catalyze each other to facilitate peptide aggregation via conformational selection.<sup>15–18</sup> On the other hand, in any scenario of rIAPP being as a catalyst or an inhibitor at any stage in the aggregation process, these seemingly controversial data suggest that rIAPP can bind to or interact with hIAPP for modulating hIAPP aggregation to some extent. However, due to the complex cross-sequence interactions between hIAPP and rIAPP, atomic-level details of the structural dynamics and mutual interaction between hIAPP and rIAPP have not been completely uncovered, while intensive experimental and computational studies have examined the effect of sequences on the structures, aggregation, and toxicity of hIAPP and rIAPP separately.<sup>8,19</sup>

Our recent experimental work has shown that hIAPP and rIAPP can interact and associate with each other to form the more and larger hybrid amyloid oligomers and fibrils.<sup>20</sup> To better probe the cross-sequence interactions and structures between hIAPP and rIAPP at atomic level, herein we systematically examined the interaction of rIAPP monomer with a series of hIAPP aggregates from monomer to pentamer using explicit-water molecular dynamics (MD) simulations. Currently, there are no atomic structures of hIAPP oligomers available, particularly from small hIAPP dimer up to pentamer at the very beginning of hIAPP aggregation. Numerous experimental and computational studies have shown that hIAPP oligomers with a transit nature can adopt different structures and sizes;<sup>21–24</sup> however, some of them contain  $\beta$ -

sheet-rich structure, which could serve as nucleation seeds for subsequent oligomerization and fibrilization.<sup>25,26</sup> Here we used a template  $\beta$ -strand–loop– $\beta$ -strand (U-shape) motif extracted from NMR-solved structures of full-length hIAPP<sub>1–37</sub> fibrils<sup>27–35</sup> to construct hIAPP oligomers. The U-shaped hIAPP monomer consists of two antiparallel  $\beta$ -strands connected by a turn, and multiple hIAPP monomers are associated with each other in an in-register way to form a parallel  $\beta$ -sheet. Such U-shaped hIAPP oligomers serve as one of the structural models for cross-seeding hIAPP–rIAPP assemblies. We realize that cross-sequence interactions between hIAPP and rIAPP resulting in cross-amyloid heteroassemblies can be involved by a wide variety of amyloid aggregates of different sizes, structures, and sequences that interact with each other through diverse binding modes, strengths, and sites between hIAPP and rIAPP, leading to a very complex energy landscape along the conformational and aggregation pathways. To better understand such complex cross-seeding behaviors between hIAPP and rIAPP, initial binding of rIAPP monomer to the template hIAPP oligomers is critical to a precursor step for the subsequent formation of hybrid hIAPP–rIAPP protofibrils and fibrils. Simulation results showed that the hIAPP oligomers can indeed interact and associate with rIAPP monomer to form stable hIAPP–rIAPP complexes, and induce its structural alternation of rIAPP to form more  $\beta$ -sheet conformations as compared to random conformation of rIAPP monomer alone in solution. More interestingly, all hIAPP oligomers exhibited a strong binding affinity to rIAPP, which may suggest some common molecular recognition features in cross-seeding, assembly, and interaction between different amyloid sequences. Our hIAPP–rIAPP heteroassembly models present possible structures and interaction models to demonstrate the existence of the rIAPP–hIAPP cross-seeding species under certain conditions. These hIAPP–rIAPP models do not necessarily exclude other structural models due to the complex polymorphic species of amyloid peptides. This work provides molecular details of hybrid hIAPP–rIAPP assemblies, leading to an improved understanding of the cross-seeding of different amyloid sequences toward amyloid aggregation and amyloid toxicity mechanisms.<sup>36,37</sup>

## MATERIALS AND METHODS

**hIAPP and rIAPP Models.** hIAPP<sub>1–37</sub> monomeric coordinates were extracted and averaged from solid-state NMR-solved structures as kindly provided by the Tycko's lab.<sup>28</sup> hIAPP<sub>1–37</sub> monomer had a  $\beta$ -strand–loop– $\beta$ -strand (U-shaped) structure containing two  $\beta$ -strands linked by a short turn, i.e.,  $\beta$ -strand (Lys1–Val17)–turn (His18–Leu27)– $\beta$ -strand (Ser28–Tyr37). The full-length hIAPP<sub>1–37</sub> peptide contains different function regions:<sup>38</sup> a N-terminal region (residues 1–19) involving membrane binding and insulin binding, an amyloidogenic region (residues 20–29), and a C-terminal region (residues 30–37) involving peptide self-association. Cys2 and Cys7 formed an intramolecular disulfide bond to stabilize the conformation at the N-termini. The N- and C-termini were capped by NH<sub>3</sub><sup>+</sup> and COO<sup>–</sup> groups, yielding a net charge of +3e at a pH of 7.4. A hIAPP<sub>1–37</sub> oligomer (from dimer to pentamer) was built by stacking hIAPP<sub>1–37</sub> monomers on top of each other in a parallel and register way, with an initial interpeptide separation of ~4.7 Å, corresponding to experimental data.<sup>28</sup> The initial structure of the rIAPP<sub>1–37</sub> monomer was built from the corresponding hIAPP<sub>1–37</sub> monomer by simply replacing side chains of six targeted

residues with His18Arg, Phe23Leu, Ala25Pro, Ile26Val, Ser28Pro, and Ser29Pro while still retaining the same backbone conformations and side chain orientations. rIAPP<sub>1–37</sub> monomer was energy minimized for 500 steps using the steepest decent method with the backbone of the peptide restrained prior to MD simulations. To build hybrid hIAPP–rIAPP assemblies, the rIAPP<sub>1–37</sub> monomer was stacked on the top of the hIAPP<sub>1–37</sub> oligomers in the same registered way as the hIAPP oligomers being constructed, which enables the overlap of side chains at the hIAPP–rIAPP interface to be maximized. Moreover, to examine the bound and unbound energetic states of rIAPP monomer in the presence and absence of hIAPP oligomers, rIAPP monomers were first extracted from the final 120 ns structures of hybrid hIAPP–rIAPP assemblies, and then subject to additional independent 30 ns MD simulations alone in the explicit water to obtain the structures and energetics at the unbound state. All simulation models were summarized in Table 1.

**Table 1. Summary of Simulation Systems with Structural Characteristics<sup>a</sup>**

system	backbone RMSD (Å)	normalized SASA* (Å <sup>2</sup> )	times (ns)
hIAPP <sub>1</sub> –rIAPP <sub>1</sub>	8.9 ± 0.6	5971.2 ± 185.4	120
extracted rIAPP			30
hIAPP <sub>2</sub> –rIAPP <sub>1</sub>	6.9 ± 0.4	7825.0 ± 175.9	120
extracted rIAPP			30
hIAPP <sub>3</sub> –rIAPP <sub>1</sub>	6.7 ± 0.3	9168.2 ± 146.3	120
extracted rIAPP			30
hIAPP <sub>4</sub> –rIAPP <sub>1</sub>	4.9 ± 0.3	10569.4 ± 164.8	120
extracted rIAPP			30
hIAPP <sub>5</sub> –rIAPP <sub>1</sub>	5.1 ± 0.3	11940.5 ± 159.1	120
extracted rIAPP			30
single rIAPP	11.9 ± 1.1	3578.9 ± 190.6	120

<sup>a</sup>All data are averaged from the last 20 ns simulations.

**Explicit-Solvent MD Simulation.** All MD simulations were performed and repeated using the NAMD package<sup>39</sup> with the CHARMM27 force field with CMAP correction<sup>40</sup> and the Gromacs package with the Gromos54a7 force field.<sup>41</sup> Each hIAPP–rIAPP assembly was solvated in a water box with a minimal margin of 15 Å from any edge of the water box to any peptide atom. Each system was neutralized by adding Cl<sup>−</sup> and Na<sup>+</sup> ions to mimic ~150 mM ionic strength. The resulting solvated and neutralized hIAPP–rIAPP systems were then subject to 5000 steps of steepest descent minimization with peptide backbone atoms harmonically constrained, followed by additional 5000 steps of conjugate gradient minimization without any constraint. The systems were then heated from 0 to 310 K by 1 ns MD simulations with peptide backbones being constrained. The production MD simulations were performed using a NPT ensemble ( $T = 310$  K and  $P = 1$  atm). The Langevin piston method with a decay period of 100 fs and a damping time of 50 fs was used to maintain a constant pressure of 1 atm, while the Langevin thermostat method with a damping coefficient of 1 ps<sup>−1</sup> was used to control the temperature at 310 K. The RATTLE method was used to constrain all covalent bonds involving hydrogen. The velocity Verlet integration was used to solve the Newtonian motion with a time step of 2 fs. Short-range van der Waals (VDW) interactions were calculated by the switch function with a twin-range cutoff at 12 and 14 Å. Long-range electrostatic

interactions were calculated using the force-shifted method with a 14 Å cutoff. The trajectories were saved every 2 ps for later analysis. All analyses were performed using tools within the CHARMM, VMD,<sup>42</sup> and code developed in-house.

**AFM Images of hIAPP–rIAPP Aggregates.** The lyophilized hIAPP and rIAPP were purchased from American Peptide Inc. (Sunnyvale, CA) and stored at −20 °C as arrived. First, both hIAPP and rIAPP were dissolved in 1,1,1,3,3,3-hexafluoro-2-propanol (HFIP), which were subsequently subject to the sonication of 30 min, followed by 30 min of centrifugation at 14 000 rpm to remove any pre-existing aggregate. The top hIAPP and rIAPP solutions were extracted and frozen with liquid nitrogen. The resulting IAPP solutions were further frozenly dried at −80 °C to obtain monomeric hIAPP and rIAPP powder. Individual 0.2 mg monomeric hIAPP and rIAPP powder was dissolved into 20 μL of DMSO and sonicated for 1 min to obtain the homogeneous IAPP monomer solutions. The resulting 20 μL of DMSO–hIAPP or DMSO–rIAPP homogeneous solution was added into 2 mL of PBS buffer of 10 mM to achieve a hIAPP/rIAPP concentration of 25 μm. The 25 μm hIAPP/rIAPP solutions were further processed by means of sonication and centrifugation to remove existing oligomers. Using the same preparation protocol, the hybrid hIAPP–rIAPP mixtures with the different concentration ratios of 25 μm:12.5 μm, 25 μm:25 μm, and 25 μm:50 μm were successfully prepared. Tapping-mode AFM was employed to monitor the morphological changes throughout the fibrillization process of pure hIAPP, pure rIAPP, and mixed hIAPP–rIAPP. Pure hIAPP/rIAPP solutions and the mixed hIAPP–rIAPP solutions were first deposited onto the cleaved mica surface for ~1 min, followed by rinsing with the deionized water three times and drying in the flow air for 5 min. Then, the tapping-mode AFM was performed in air using the Nanoscope III multimode scanning probe microscope (Veeco Corp., Santa Barbara, CA) with a 15 μm E scanner. Commercial Si cantilevers with an elastic modulus of 40 N m<sup>−1</sup> and a typical scan rate of 1.0–2.0 Hz with a vertical tip oscillation frequency of 250–350 kHz were employed to obtain all the final 512 × 512 pixel AFM images.

## RESULTS AND DISCUSSION

To validate the convergence of our simulation models, each hIAPP–rIAPP system was run, repeated, and cross-checked for 120 ns using the two different force fields of CHARMM27 and Gromos54a7. For all the simulated systems, both CHARMM27 and Gromos54a7 force fields reproduced similar structural characteristics of hIAPP–rIAPP heteroassemblies (Figure 1). Within 120 ns simulations, the rIAPP was able to associate with hIAPP peptides, with the U-shaped β-sheet structures of hIAPP being largely retained in the higher-order heteroassemblies. Meanwhile, we also observed some minor structural and dynamic deviations, particularly in the terminal regions. It appears that Gromos54a7-produced conformations have relatively higher structural flexibility at both C-/N-terminus, presumably due to the use of the united atom models. Due to the high reproducibility of our simulation models, below we used the CHARMM trajectories to conduct all data analysis.

**Heteroassociation between hIAPP and rIAPP.** Figure 1 shows MD snapshots of hybrid hIAPP–rIAPP assemblies of varied sizes averaged from the last 20 ns of 120 ns MD trajectories extracted from the CHARMM27 and Gromos54a7 force fields. The overall hIAPP–rIAPP structures obtained from the two force fields exhibited considerable consistency

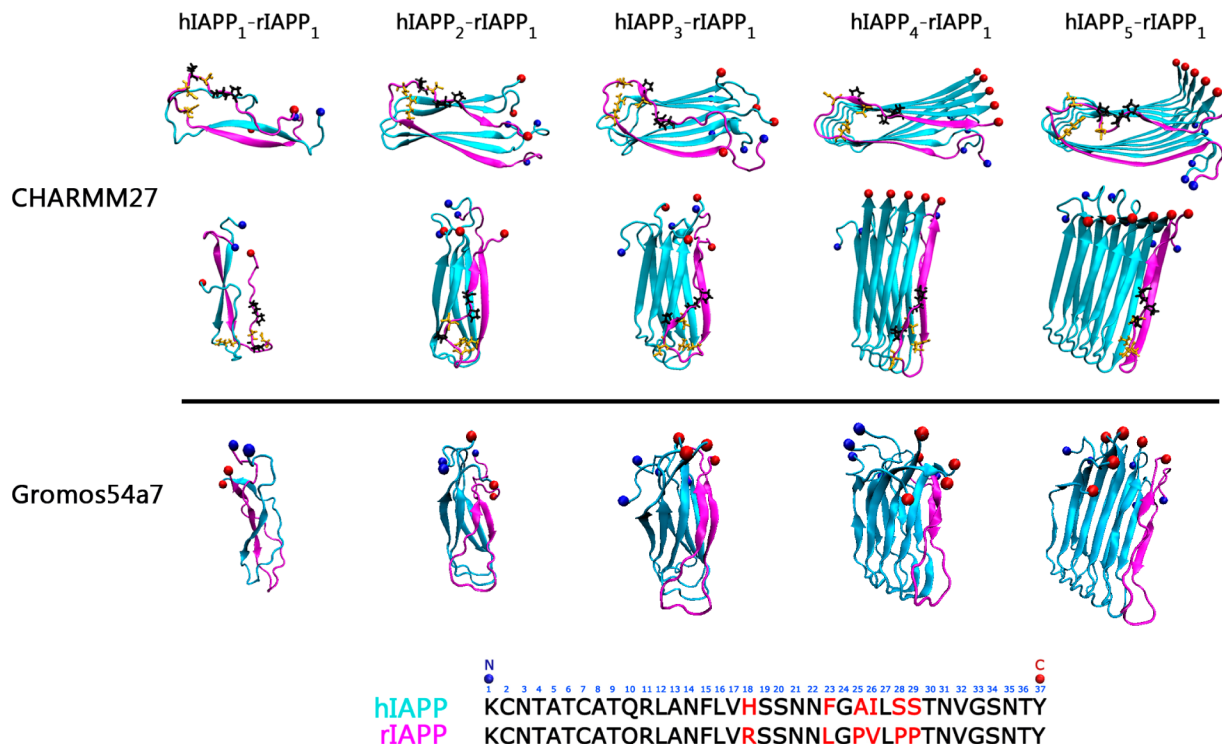


**Figure 1.** MD snapshots (top and side views) of hybrid hIAPP–rIAPP aggregates from hIAPP<sub>1</sub>–rIAPP<sub>1</sub> to hIAPP<sub>5</sub>–rIAPP<sub>1</sub> averaged from the last 20 ns simulations using both CHARMM27 and Gromos54a7 force fields. Six residues of rIAPP at the positions of 18, 23, 25, 26, 28, and 29 are present by CPK to highlight sequence difference between hIAPP and rIAPP. Color scheme: proline (black), arginine, leucine, and valine (orange). C-termini and N-termini are presented by red and blue beads for guiding the eyes, and water and ions are removed for clarity.

with some minor structural differences existing in the terminal regions, suggesting that the force fields have little influence on the  $\beta$ -structure-dominant systems. The overall potential energies for all hIAPP–rIAPP complex systems were stabilized after 60 ns (data not shown), ensuring that the systems are properly equilibrated. At first glance over the 120 ns MD trajectories, all simulations showed that rIAPP monomer was able to steadily associate with hIAPP monomer or oligomers, and overall structures of particular high-order hybrid assemblies were largely preserved with only some local changes. This was further confirmed by Rg (radius of gyration). As shown in Figure 2a, except for hIAPP<sub>1</sub>:rIAPP<sub>1</sub> complex, Rg values of other hIAPP–rIAPP complexes from hIAPP<sub>2</sub>:rIAPP<sub>1</sub> to hIAPP<sub>5</sub>:rIAPP<sub>1</sub> almost stayed leveled or experienced a very small decrease by 1–2 Å. These high-order hIAPP–rIAPP complexes tended to retain initial extended  $\beta$ -strand-like conformations with certain degrees of twisting between adjacent peptides. In these simulations, subtle fluctuations of Rg values also indicate that the systems have reached equilibrium. Meanwhile, the small hIAPP<sub>2</sub>:rIAPP<sub>1</sub> complex experienced relatively large fluctuation and decrease in Rg ranging from 18 to 16 Å. This became more pronounced for rIAPP monomer, whose Rg sharply dropped from 17 to 11 Å, suggesting that rIAPP monomer prefers to adopt a disordered and frizzy conformation in solution, in good agreement with the previous experimental and computational observations.<sup>43,44</sup> Examination of the extent of peptide conformations reveals that the most favorable hIAPP–rIAPP complexes to form hybrid amyloids should be the extended structures with the larger Rg.

The time series of the backbone RMSD of different sizes of hIAPP–rIAPP assemblies were used to characterize their relative structural stabilities (Figure 2b). It can be clearly seen

that a single rIAPP monomer without binding to any hIAPP oligomer gave the largest RMSD up to 11.9 Å and consistent RMSD fluctuation of ~1.1 Å during 120 ns simulations. When the rIAPP monomer bound to hIAPP monomer, dimer, and trimer, the averaged RMSDs of hIAPP<sub>1</sub>–rIAPP, hIAPP<sub>2</sub>–rIAPP, and hIAPP<sub>3</sub>–rIAPP heteroassemblies were greatly reduced to 8.9, 6.9, and 6.7 Å, respectively. This trend became more pronounced as the rIAPP monomer bound to hIAPP tetramer and pentamer, which gave rise to small and steady RMSDs of 4.9 and 5.1 Å during the simulations. In all heteroassemblies, no immediate dissociation of rIAPP monomer from hIAPP peptides was observed. hIAPP seeds from dimer to pentamer in the heteroassemblies were well maintained for their  $\beta$ -strands and U-shaped conformation. This indicates that the U-shape conformation of hIAPP, which is highly stable, makes it possible for the  $\beta$ -strand of rIAPP to interact with the  $\beta$ -sheet of hIAPP peptides, although rIAPP monomer adopts a less perfect U-shape and less populated  $\beta$ -structure particularly at the C-terminal region. MD trajectories showed that overall conformational changes of these heteroassemblies mainly came from peptide twists between neighboring  $\beta$ -strands and the loss of  $\beta$ -strand of rIAPP. The observation of peptide twisting is consistent with the NMR-solved structure of hIAPP fibrils<sup>28</sup> and could represent a prerequisite for the optimization of side chain interaction and conformation for incorporation of oligomers into fibrils. This observation was also supported by the fact that rIAPP monomer generally exhibited the relatively larger residue-based RMSF (root-mean-square fluctuation) than hIAPP oligomers across all residues (Figure 2c). The increased RMSF of rIAPP appears to be correlated with solvent accessible surface area (SASA) of rIAPP, shown in Figure 2d. This is not surprising,

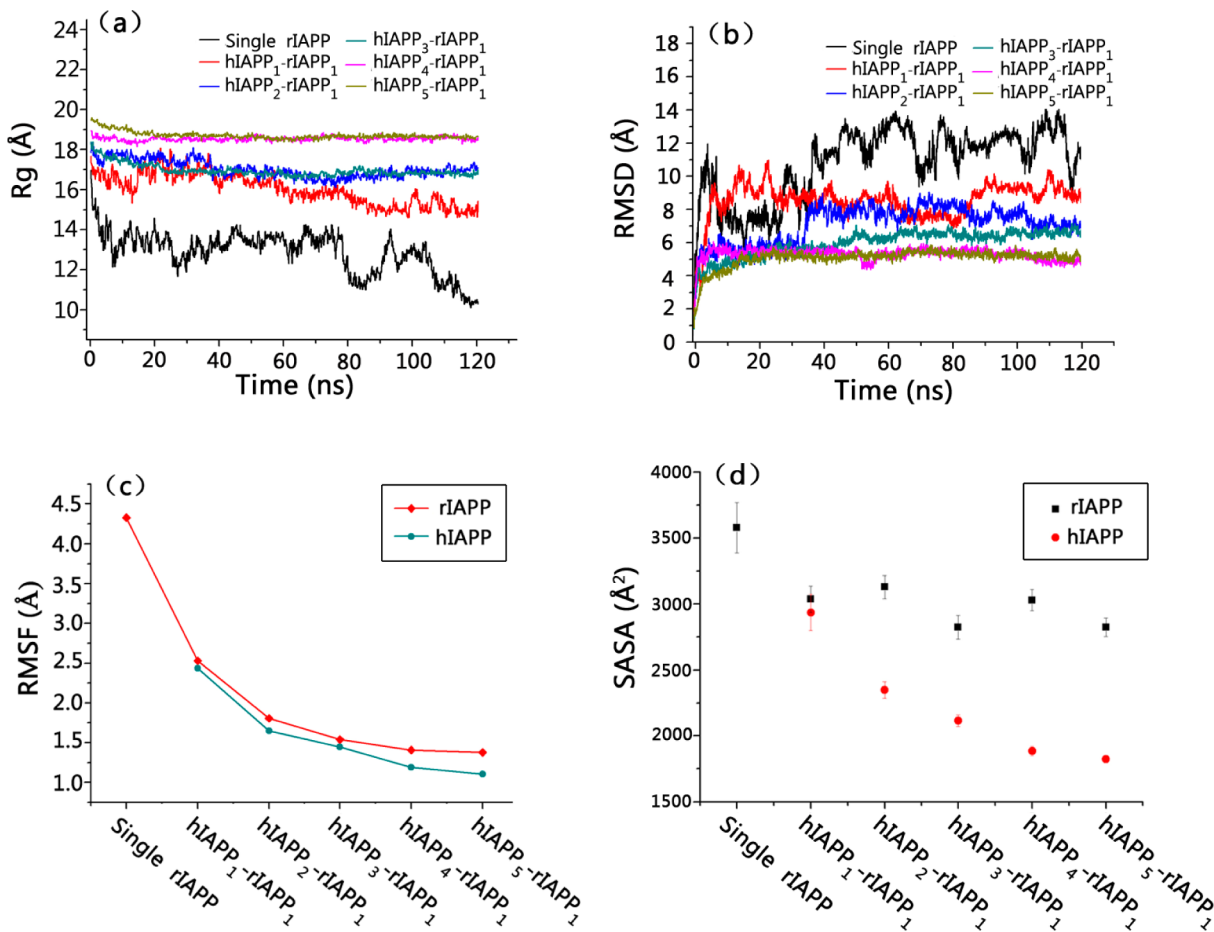


**Figure 2.** Geometric and structural characterization of the hybrid hIAPP–rIAPP assemblies. (a)  $R_g$ , (b) backbone RMSD, (c) residue-based RMSF, and (d) SASA of hybrid hIAPP–rIAPP aggregates. The RMSF and SASA data are averaged from the last 20 ns simulations.

because rIAPP bound at the edge of hIAPP peptides was large exposed to the solvent. Consistently, the residues of the inner peptides and the central residues of the peptides were less solvent-exposed than those of the outer peptides and the edge residues, leading to the smaller RMSF values as well. In addition, the increased number of hIAPP peptides will enhance their self-association, leading to the more stabilized hIAPP structures. This can be evidenced by the less structural fluctuation of hIAPP peptides (RMSF in Figure 2c) and the relatively small twisting angles between the adjacent hIAPP peptides (MD snapshots in Figure 1). The more stable hIAPP oligomers are expected to provide the better structural templates for facilitating the pair-to-pair association with rIAPP.

Our results provide the evidence that hIAPP monomer and oligomers can interact with conformationally similar rIAPP to form stable complexes and to coassemble into heterogeneous structures. While some small heteroassemblies exhibited a rather larger conformational change and flexibility, the overall structural stability of heteroassemblies increases as the size of hIAPP seeds. This suggests that hIAPP seeds of different sizes, even hIAPP dimer, can indeed cross-seed rIAPP to mutually enhance the structural integrity and the  $\beta$ -sheet percentage of both hIAPP and rIAPP peptides, which could promote self-aggregation and facilitate amyloid fibril formation. It is likely that conformational similarity and flexibility of hIAPP and rIAPP enable hetero- and self-association of hIAPP and rIAPP in a competitive manner. Consistent with our mutual conformational selection that structural similarities can cause

amyloids composed of different sequences, Hansmann and co-workers have reported that  $A\beta_{15-40}$  and hIAPP<sub>10-35</sub> that adopted similar U-shaped conformations can interact with each other to form heteroassemblies.<sup>36,37</sup> Similar cross-sequence interactions of different amyloid sequences were also observed between full-length hIAPP and its Y37L mutant,<sup>37</sup>  $A\beta_{42}$  and tau,<sup>45,46</sup>  $A\beta$  and IAPP,<sup>47,48</sup> tau and  $\alpha$ -synuclein,<sup>49</sup> and between different microtubule binding repeats of tau.<sup>50-52</sup> The cross-seeding of different amyloid sequences requires mutual conformational selection of both sequences to adopt similar conformations that allow specific and selective recognition in amyloid growth to be achieved.<sup>18</sup>

**Increase of the  $\beta$ -Sheet Population of the Hetero-assemblies.** As a control, simulations of a single rIAPP monomer in solution clearly showed that rIAPP monomer largely lost its original U-shaped conformation and transformed into a disordered structure containing mixed coil, bend, turn, and  $\beta$ -structure (12.6%). This suggests that rIAPP monomer is not prone to form dominant  $\beta$ -structure in solution. This structural characteristic is reasonably consistent with experimental observation that rIAPP monomer mainly adopts the disordered structures in solution.<sup>13,21,23,53-56</sup> However, when rIAPP was coassembled with hIAPP peptides to form heteroassemblies, visual inspection of 120 ns MD trajectories showed that rIAPP monomer was able to retain the U-shaped conformation and the  $\beta$ -structure to some extent. Figure 3a shows the secondary structure of different hIAPP–rIAPP assemblies as a function of time, while Figure 3b quantitatively

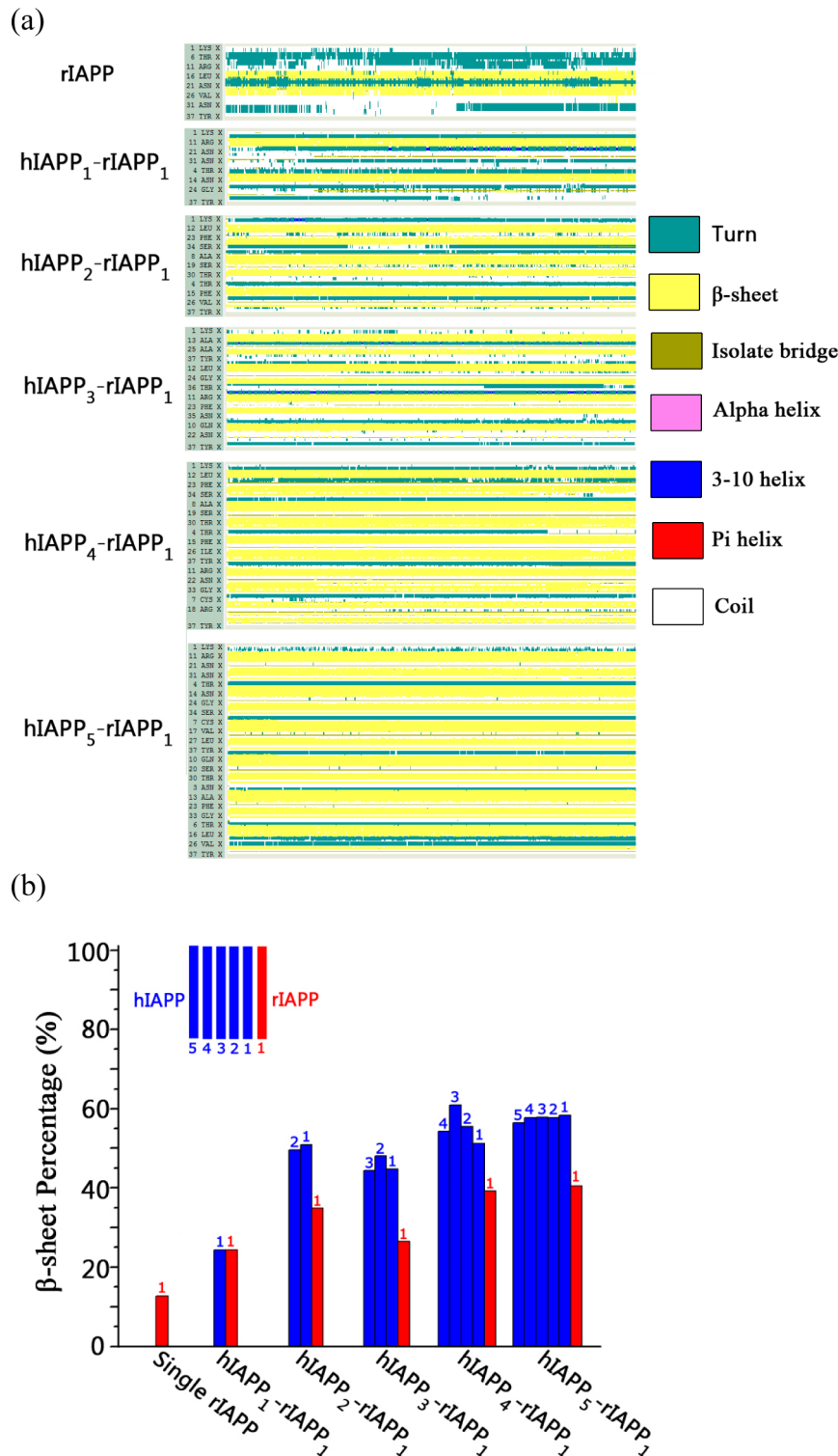


**Figure 3.** (a) Time evolution of secondary structure and (b) averaged  $\beta$ -sheet percentages for all hIAPP–rIAPP heteroassemblies and single rIAPP from last 20 ns simulations, as calculated by the stride algorithm.

measures the  $\beta$ -sheet content of each individual hIAPP and rIAPP peptide in all heteroassemblies using the stride algorithm.<sup>42</sup> In all hIAPP–rIAPP heteroassemblies, the U-shaped structure of the rIAPP monomer was disturbed somehow, and the  $\beta$ -sheet population of rIAPP was increased from 12.6% in the absence of hIAPP to 24.5, 34.9, 26.5, 39.2, and 40.6% when bound to hIAPP monomer, dimer, trimer, tetramer, and pentamer, respectively. Figure 3a showed that

rIAPP partially lost its initial C-terminal  $\beta$ -strand containing four different residues from the hIAPP while still largely maintaining approximately three to five residues in the form of  $\beta$ -strand at the N-terminal. It is conceivable that the increased trend of  $\beta$ -sheet content of rIAPP can be attributed to the enhanced interpeptide interactions between rIAPP and hIAPP. The presence of hIAPP peptides greatly reduces the degree of

freedom for rIAPP conformational variation, thus stabilizing the U-shaped  $\beta$ -sheet structure for heteroassemblies.

Meanwhile, a secondary structure population analysis of the hIAPP peptides in all heteroassemblies showed that, almost independent of hIAPP sizes, the parallel cross- $\beta$ -structures of hIAPP peptides were largely preserved, and their  $\beta$ -sheet populations remained almost unchanged (44.4–60.9%) from their initial structures during the entire simulations (Figure 3b). Dupuis et al.<sup>26</sup> reported that hIAPP peptides formed a  $\beta$ -strand-rich dimer containing 15–25%  $\beta$ -structure, consistent with the  $\beta$ -structure content of our hybrid hIAPP–rIAPP dimer of 24.4%. The  $\beta$ -structure population of the inner hIAPP strands was slightly higher than that of the outer hIAPP strands due to the less surface exposure to solvent and the more confinement of strand movement. A number of studies have shown that the  $\beta$ -sheet structure is a general structural feature of amyloid nucleus and fibrils.<sup>32,57,58</sup> The rIAPP and hIAPP may compete with the cooperative association among self- and heteroassociation. Considering that rIAPP adopts less  $\beta$ -sheet-rich structure, heteroassociation between hIAPP and rIAPP needs more entropy and enthalpy cost than self-association of hIAPP to form  $\beta$ -sheet-rich protofibrils and fibrils, leading to less efficiency of interfacial interaction for heteroassociation. This cross-interaction could provide a possible explanation that experimentally rIAPP must be presented by 10-fold excess to enable effective interaction with hIAPP for amyloid formation.<sup>13</sup> For the same reason, simulation results may also interpret experimental observation by ours and Middleton et al.<sup>14</sup> that coincubation of rIAPP with hIAPP lengthens the lag phase at the early stage of peptide aggregation, because the bound rIAPP has less perfect U-shaped  $\beta$ -strand structure and limited structural flexibility to effectively accommodate other hIAPP or rIAPP by optimal side-by-side  $\beta$ -sheet association; thus, it will take a longer time to form a heteronucleus.

**Interpeptide Interactions at the hIAPP–rIAPP Interface.** Both hIAPP and rIAPP are amphiphilic peptides. Hydrogen bonds and hydrophobic contacts between hIAPP and rIAPP play critical roles in controlling the conformational dynamics and bound state of heteroassemblies. Simulation results showed that, for all heteroassemblies, both hydrophobic contacts and hydrogen bonds at the hIAPP–rIAPP interface were almost homogeneously distributed along two  $\beta$ -strands, suggesting that both interactions work cooperatively to achieve more stable interactions between rIAPP and hIAPP. Meanwhile, Figure 4 showed that the total numbers of the hydrogen bonds and hydrophobic contacts at the interface exhibited an ascending tendency from hIAPP<sub>1</sub>–rIAPP<sub>1</sub> to hIAPP<sub>3</sub>–rIAPP<sub>1</sub>, and reached the summit of ~37.5 for hIAPP<sub>4</sub>–rIAPP<sub>1</sub> and hIAPP<sub>5</sub>–rIAPP<sub>1</sub>, implying that the interaction at the interface became stronger as the size of the hybrid oligomers increased. Generally, the more hydrogen bonds are formed relative to hydrophobic contacts. This probably because the large percentage of  $\beta$ -strand structures at the hIAPP–rIAPP interface, as evidenced by secondary structure analysis, requires a large number of backbone–backbone hydrogen bonds to be held for its stability and integrity. These hydrogen bonds tightly encompassed a solvated pore along the fibril axis as well. Different from the naturally folding proteins, the evenly distributed hydrophobic amino acids along hIAPP and rIAPP sequences were only capable of forming hydrophobic contacts at several specific sites, but hydrophobic contacts cannot be neglected due to its complementary function in stabilizing the assemblies.

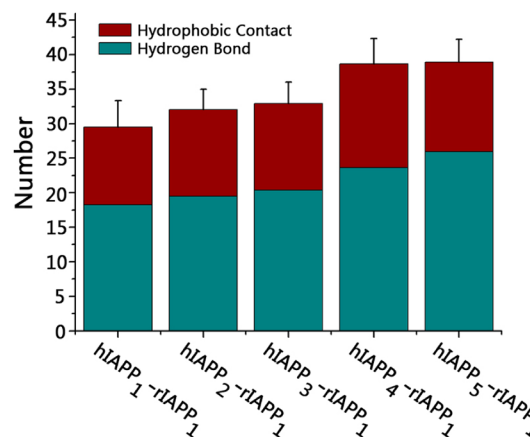


**Figure 4.** Number of hydrogen bonds and hydrophobic contacts at the hIAPP–rIAPP interface for different heteroassemblies averaged from the last 20 ns simulations. A hydrogen bond is defined if the distance between the donor D and acceptor A is less than 3.2 Å and the angle D–H…A is larger than 120°. A hydrophobic contact is identified as a center distance between two hydrophobic residues of less than 6.5 Å.

It is also important to quantify the energy contribution of each residue of rIAPP to the hIAPP–rIAPP interactions, which will provide more quantitative determination of possible important binding residues and binding sites for heteroassociation. Figure 5 showed the interaction energy maps between each residue of rIAPP monomer and hIAPP peptides. Although the residue<sub>rIAPP</sub>–hIAPP interactions were highly nonhomogeneous and strongly relied on the size of hIAPP, rIAPP still showed some similar interaction patterns upon associating with hIAPP peptides. Two preferential regions of the N-terminal  $\beta$ -structure region (Cys7–Ser20) and C-terminal  $\beta$ -structure region (Pro26–Tyr37) were identified to have the stronger interactions between rIAPP residues and hIAPP peptides. Meanwhile, the N-terminal  $\beta$ -structure region of rIAPP presented the higher interfacial interaction than the C-terminal  $\beta$ -structure region. This because three prolines known as a  $\beta$ -sheet breaker at the C-termini of rIAPP caused a loss of compact stacking with its counterpart of hIAPP, giving rise to the relatively lower interaction energies at this region. In addition, for hIAPP<sub>1</sub>–rIAPP<sub>1</sub>, hIAPP<sub>2</sub>–rIAPP<sub>1</sub>, and hIAPP<sub>3</sub>–rIAPP<sub>1</sub>, some interaction energies were lost at the Asn35–Tyr37 region. The visual inspection of trajectories provided a consistent view of the interacting modes in the Asn35–Tyr37 region; i.e., hIAPP monomer, dimer, and trimer lost their initial  $\beta$ -structures in this region to a greater degree than hIAPP tetramer and pentamer, which may account for a much weaker interaction mode. As a consequence, it can be expected that the disordered loop structures at C-termini of small hIAPP oligomers would be a negative factor for the formation of a stable and compact hIAPP–rIAPP assembly.

**Bound and Unbound States of rIAPP.** Our simulation results have shown that rIAPP monomer in the absence and presence of hIAPP seeds adopted different conformations in the unbound and bound states, respectively. To further quantify the energy states of bound and unbound rIAPP monomers, we extracted final structures of rIAPP monomer from all heteroassemblies at the bound state, and then conducted additional 30 ns MD simulations to study the conformational dynamics and energy state of rIAPP monomer alone at the unbound state. In all cases, the conformations collected from different rIAPP monomers at the equilibrium unbound state

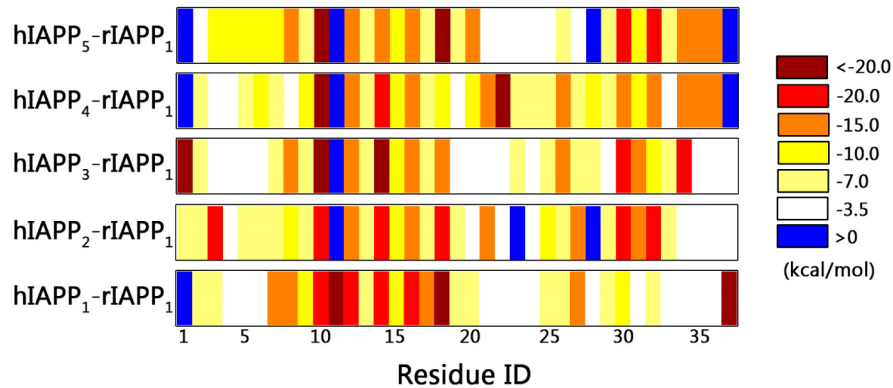


**Figure 5.** Residue-based interaction energy map between individual residues of rIAPP and its counterpart hIAPP peptides.

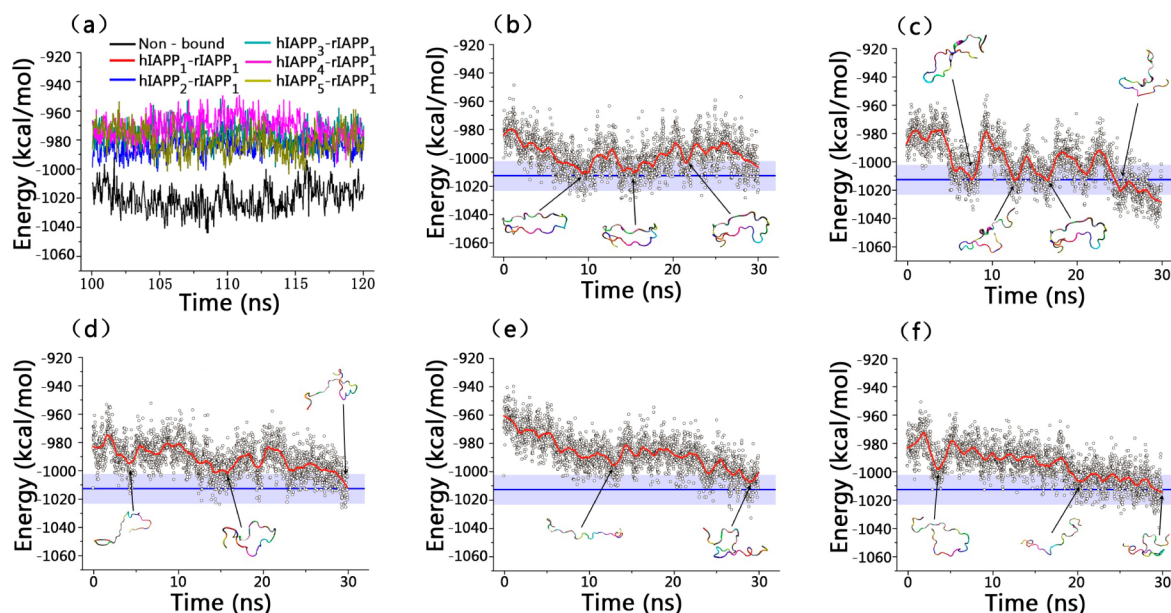


**Figure 6.** (a) Conformational energies of rIAPP peptides in the absence and presence of hIAPP peptides obtained from the last 20 of 120 ns simulations. Conformational energy pathways of the unbound rIAPP extracted from (b) hIAPP<sub>1</sub>-rIAPP<sub>1</sub>, (c) hIAPP<sub>2</sub>-rIAPP<sub>1</sub>, (d) hIAPP<sub>3</sub>-rIAPP<sub>1</sub>, (e) hIAPP<sub>4</sub>-rIAPP<sub>1</sub>, and (f) hIAPP<sub>5</sub>-rIAPP<sub>1</sub>, respectively. For comparison, in parts b–f, the average conformational energy of rIAPP in solution ( $-1013.2 \text{ kcal/mol}$ ) and its standard deviation ( $11.3 \text{ kcal/mol}$ ) are denoted by the blue lines and the surrounding light blue regions, respectively. All conformational energies are calculated using the GBMV method.

appeared to be not much different from the conformation of rIAPP in its free form in solution, i.e., the unbound rIAPP adopted a mixed conformation of random coil and helix. CD experiments confirmed that rIAPP monomer did not adopt a well-ordered structure in aqueous solution.<sup>13</sup> Such similar conformations further suggest that the binding process may be a reasonable representation of the natural process. More importantly, as shown in Figure 6a, the conformational energies of rIAPP monomers at the bound state were consistently higher than those of rIAPP monomers at the unbound state. At the bound state, the presence of hIAPP greatly reduces the conformational change and flexibility of rIAPP, resulting in a large reduction in entropy. The loss of entropy at the bound state was partially compensated by increased interfacial interactions induced by hIAPP. Competition between the loss of entropy and the gain of enthalpy would lead to the higher energy state of rIAPP at the interface as compared to the unbound state.

More importantly, as shown in Figure 6b–f, energy trajectories of the rIAPP monomers starting from the bound

state displayed a gradual energy loss from the high-energy state to the low-energy state. The overall energy difference between the bound rIAPP and the unbound rIAPP is a sum of many small energy differences between many different transition states. Along the reverse pathways from the unbound rIAPP to the bound hIAPP consisting of a number of transition states (each dot in Figure 6 represents a configurational transition state), since the energy difference between these transition states is rather small, it is possible that the unbound rIAPP would not encounter large energy barriers to interact with or adsorb on the hIAPP, becoming the bound rIAPP. It should be noted that when transiting from the unbound state to the bound state, the conformational energy change of rIAPP alone seems to be unfavorable, but this unfavorable energy change can be fairly compensated by the favorable interpeptide interactions between hIAPP and rIAPP, which will eventually drive the formation of the hIAPP–rIAPP complexes under certain conditions. Moreover, in Figure 6b–f, the unbound rIAPPs adopted different saddle-point conformations along the whole procedure, indicating that, through conformational

changes, these polymorphic rIAPP monomers could overcome many small energy barriers and pass through different reversible pathways to achieve the cross-seeding with hIAPP. Thus, the cross-seeding of rIAPP could be accessible via a conformation-independent process. As long as hIAPP oligomers provide the suitable templates, rIAPP can gradually adjust its conformation and convert to a seed-favorable structure for promoting the cross-seeding under certain conditions. It could also be expected that the cross-seeding of rIAPP with hIAPP has no special demand on the specific conformation of rIAPP, and different conformations of rIAPP can serve as potential candidates for the cross-seeding with hIAPP upon proper structural changes.

#### AFM Study of Cross-Aggregation of hIAPP and rIAPP.

Parallel to simulation results, AFM was employed to monitor the aggregation process when incubating hIAPP and rIAPP together at different molar ratios of hIAPP:rIAPP of 1:0.5, 1:1, and 1:2, as compared with those of fibrils formed by pure hIAPP and pure rIAPP in solution. AFM images recorded at the end point of 20 h showed that pure hIAPP formed typical amyloid fibrils, while pure rIAPP did not produce any fibril instead of many amorphous particles (Figure 7). Our recent

of homoassemblies by pure hIAPP. The relative slow kinetics of fibril formation by hIAPP and rIAPP mixtures is attributed to the lesser efficiency for rIAPP to structurally sample and transit to  $\beta$ -structures for peptide aggregation. The final ThT fluorescence intensity, used for measuring the amount of amyloid fibrils being formed, of the hIAPP-rIAPP mixtures at various ratios (1:0.5, 1:1, and 1:2) consistently increased by 18.5–33.4% as compared to that of pure hIAPP. Considering that all mixed samples contained the same amount of hIAPP (25  $\mu$ M) but different rIAPP amounts while rIAPP itself did not form fibrils, the increased fluorescence intensities did not come from hIAPP fibrils only, and instead came from newly formed hybrid hIAPP-rIAPP fibrils, consistent with the AFM images of dense fibrils. We also found that the hIAPP:rIAPP mixture (1:1, 50  $\mu$ M) did not form more fibrils than pure hIAPP (50  $\mu$ M). This indicates that cross-sequence interaction between rIAPP and hIAPP is not as equally effective as homosequence interaction between pure hIAPP. These results provide additional evidence that hIAPP can seed fibril formation by rIAPP at all concentrations examined, but the cross-sequence barriers may also exist due to the sequence-induced polymorphic structures of peptides, which makes it difficult for different sequences to specifically and selectively interact with each other.

#### CONCLUSIONS

The cross-sequence interactions between different amyloid sequences play a crucial role in fundamental understanding of amyloid formation and toxicity mechanisms but also in practical development of new drugs against amyloid diseases. Here we employ MD simulations and AFM experiments to gain atomic insights into the cross-sequence interaction between hIAPP and rIAPP at the early stage of peptide aggregation. MD results show that hIAPP oligomers (even as small as hIAPP dimer) can strongly interact with conformationally similar rIAPP to form stable complexes and coassemble into heterogeneous aggregates. This indicates that the heteroassociation underlying cross-sequence interaction between hIAPP and rIAPP most likely occurs through their similar U-shaped conformation as an amyloid self-recognition domain. As compared to the unstructured conformation of rIAPP alone in solution, the presence of hIAPP seeds not only stabilizes the U-shaped  $\beta$ -structure of rIAPP to a large extent, despite being not as perfect as its counterpart of hIAPP, but also greatly reduces the conformational change and flexibility of rIAPP, resulting in a large reduction in entropy. The loss of entropy at the bound state was partially compensated by increased interfacial interactions induced by hIAPP, leading to the higher energy state of rIAPP at the bound state relative to the unbound state. Experimentally, with coincubation of hIAPP with rIAPP at various hIAPP:rIAPP ratios of 1:0.5, 1:1, and 1:2, AFM and ThT data showed significantly thicker and more fibrils, with fibril morphologies similar to those formed by pure hIAPP, confirming that hIAPP can seed fibril formation by rIAPP at all concentrations examined. We should also note that although the rIAPP and hIAPP may compete with each other to form self- and heteroassemblies, due to the less perfect  $\beta$ -sheet-rich structure of rIAPP, heteroassociation between hIAPP and rIAPP would need more entropy and enthalpy cost than self/homoassociation of hIAPP to form  $\beta$ -sheet-rich protofibrils and fibrils; thus, heteroassociation is less efficient for interfacial interactions and peptide self-assembly than self/homoassociation. This work highlights the importance of the cross-seeding

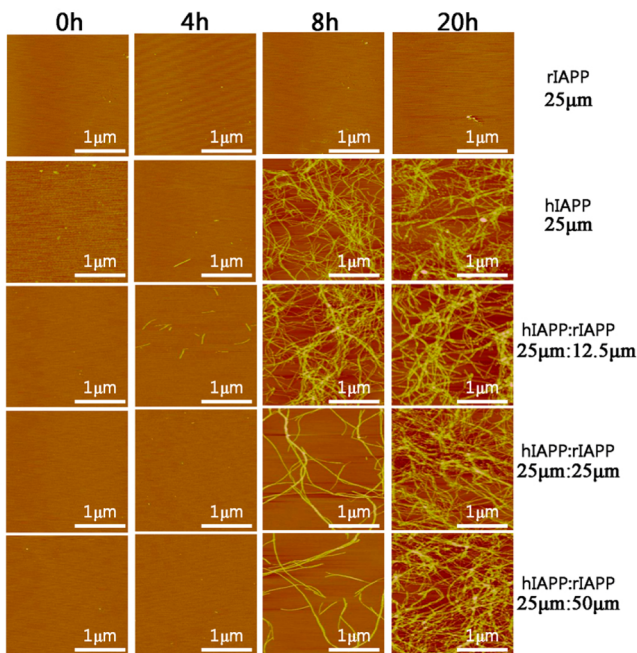


**Figure 7.** AFM images of pure rIAPP, pure hIAPP, and mixed heteroassemblies at hIAPP:rIAPP molecular ratios of 25  $\mu$ M:12.5  $\mu$ M, 25  $\mu$ M:25  $\mu$ M, and 25  $\mu$ M:50  $\mu$ M at 0, 4, 8, and 20 h, respectively.

ThT data also confirmed that hIAPP showed a typical amyloid fibrillation process starting with a lag phase of  $\sim$ 3.5 h, followed by a growth phase to a final stable plateau, while rIAPP showed no change in ThT signal.<sup>20</sup> As shown in Figure 7, a close AFM inspection of amyloid fibrillation by hIAPP-rIAPP mixtures revealed that, at 8 h, hIAPP and rIAPP mixtures at different molar ratios produced less amyloid (proto)fibrils than pure hIAPP. However, as the incubation time increased to 20 h, the end product of mature fibrils by hIAPP-rIAPP mixtures displayed long, dense, and branched fibril morphologies similar to pure hIAPP. This could be due to the fact that the formation of large heteroassemblies (protofibrils and mature fibrils) usually requires a much longer time than that

of different sequences with similar conformations for achieving heteroaggregation.

We should note that, alternative to the simulation of the end-product of hIAPP–rIAPP aggregates in our models, simulating the dynamic folding and self-assembly process of hIAPP and rIAPP mixtures, with both peptides starting with random coil conformations, can provide different aspects of kinetics aggregation pathways and structural transition along the pathway. Such models and simulations usually require different sampling techniques (e.g., replica-exchange MD, replica-exchange Monte Carlo, and configuration-biased Monte Carlo) and molecular models (e.g., coarse-grained peptide model, implicit solvent model, and dissipative particle dynamics) to capture the self-assembling and structural transition behaviors of peptides at the longer time scale and the large length scale.

## AUTHOR INFORMATION

### Corresponding Author

\*E-mail: zhengj@uakron.edu. Phone: (330) 972-2096.

### Author Contributions

#M.Z. and R.H. contributed equally to this work.

### Notes

The authors declare no competing financial interest.

## ACKNOWLEDGMENTS

We thank Dr. Robert Tycko for providing the atomic coordinates of the hIAPP fibril models. J.Z. acknowledges financial support from NSF grants (CAREER Award CBET-0952624 and CBET-1158447). G.L. acknowledges financial support from Natural Science Foundation Project of Chongqing CSTC (cstc2012gggjhz10003). We thank Eli Newby (Hudson High School, Ohio) for the construction of some models. This study utilized (in part) the high performance of the Anton cluster at the National Resource for Biomedical Supercomputing.

## REFERENCES

- (1) Khemtémourian, L.; Killian, J. A.; Höppener, J. W. M.; Engel, M. F. M. Recent Insights in Islet Amyloid Polypeptide-Induced Membrane Disruption and Its Role in Beta-Cell Death in Type 2 Diabetes Mellitus. *Exp. Diabetes Res.* **2008**, *2008*, 1–9.
- (2) Kapurniotu, A. Amyloidogenicity and Cytotoxicity of Islet Amyloid Polypeptide. *Biopolymers* **2001**, *60*, 438–459.
- (3) Cao, P.; Marek, P.; Noor, H.; Patsalo, V.; Tu, L.-H.; Wang, H.; Abedini, A.; Raleigh, D. P. Islet Amyloid: From Fundamental Biophysics to Mechanisms of Cytotoxicity. *FEBS Lett.* **2013**, *587*, 1106–1118.
- (4) Meredith, S. C. Protein Denaturation and Aggregation. Cellular Responses to Denatured and Aggregated Proteins. *Ann. N. Y. Acad. Sci.* **2006**, *1066*, 181–221.
- (5) Butterfield, S. M.; Lashuel, H. A. Amyloidogenic Protein-Membrane Interactions: Mechanistic Insight from Model Systems. *Angew. Chem., Int. Ed.* **2010**, *49*, 5628–5654.
- (6) Stefani, M. Biochemical and Biophysical Features of Both Oligomer/Fibril and Cell Membrane in Amyloid Cytotoxicity. *FEBS J.* **2010**, *277*, 4602–4613.
- (7) Weise, K.; Radovan, D.; Gohlke, A.; Opitz, N.; Winter, R. Interaction of Hiapp with Model Raft Membranes and Pancreatic Beta-Cells: Cytotoxicity of Hiapp Oligomers. *ChemBioChem* **2010**, *11*, 1280–1290.
- (8) Brender, J. R.; Salamekh, S.; Ramamoorthy, A. Membrane Disruption and Early Events in the Aggregation of the Diabetes Related Peptide Iapp from a Molecular Perspective. *Acc. Chem. Res.* **2012**, *45*, 454–462.
- (9) Last, N. B.; Rhoades, E.; Miranker, A. D. Islet Amyloid Polypeptide Demonstrates a Persistent Capacity to Disrupt Membrane Integrity. *Proc. Natl. Acad. Sci. U.S.A.* **2011**, *108*, 9460–9465.
- (10) Cleary, J. P.; Walsh, D. M.; Hofmeister, J. J.; Shankar, G. M.; Kuskowski, M. A.; Selkoe, D. J.; Ashe, K. H. Natural Oligomers of the Amyloid-[Beta] Protein Specifically Disrupt Cognitive Function. *Nat. Neurosci.* **2005**, *8*, 79–84.
- (11) Goedert, M. Alpha-Synuclein and Neurodegenerative Diseases. *Nat. Rev. Neurosci.* **2001**, *2*, 492–501.
- (12) Gilead, S.; Gazit, E. The Role of the 14–20 Domain of the Islet Amyloid Polypeptide in Amyloid Formation. *Exp. Diabetes Res.* **2008**, *2008*, 256954.
- (13) Cao, P.; Meng, F.; Abedini, A.; Raleigh, D. P. The Ability of Rodent Islet Amyloid Polypeptide to Inhibit Amyloid Formation by Human Islet Amyloid Polypeptide Has Important Implications for the Mechanism of Amyloid Formation and the Design of Inhibitors. *Biochemistry (Moscow)* **2010**, *49*, 872–881.
- (14) Middleton, C. T.; Marek, P.; Cao, P.; Chiu, C.-c.; Singh, S.; Woys, A. M.; de Pablo, J. J.; Raleigh, D. P.; Zanni, M. T. Two-Dimensional Infrared Spectroscopy Reveals the Complex Behaviour of an Amyloid Fibril Inhibitor. *Nat. Chem.* **2012**, *4*, 355–360.
- (15) Yu, X.; Luo, Y.; Dinkel, P.; Zheng, J.; Wei, G.; Margittai, M.; Nussinov, R.; Ma, B. Cross-Seeding and Conformational Selection between Three- and Four-Repeat Human Tau Proteins. *J. Biol. Chem.* **2012**, *287*, 14950–14959.
- (16) Dinkel, P. D.; Siddiqua, A.; Huynh, H.; Shah, M.; Margittai, M. Variations in Filament Conformation Dictate Seeding Barrier between Three- and Four-Repeat Tau. *Biochemistry (Moscow)* **2011**, *50*, 4330–4336.
- (17) Andreetto, E.; Yan, L.-M.; Tatarek-Nossol, M.; Velkova, A.; Frank, R.; Kapurniotu, A. Identification of Hot Regions of the A $\beta$ -Iapp Interaction Interface as High-Affinity Binding Sites in Both Cross- and Self-Association. *Angew. Chem., Int. Ed.* **2010**, *49*, 3081–3085.
- (18) Ma, B.; Nussinov, R. Selective Molecular Recognition in Amyloid Growth and Transmission and Cross-Species Barriers. *J. Mol. Biol.* **2012**, *421*, 172–184.
- (19) Morrissey-Andrews, A.; Shea, J.-E. Simulations of Protein Aggregation: Insights from Atomistic and Coarse-Grained Models. *J. Phys. Chem. Lett.* **2014**, *5*, 1899–1908.
- (20) Hu, R.; Zhang, M.; Patel, K.; Wang, Q.; Chang, Y.; Gong, X.; Zhang, G.; Zheng, J. Cross-Sequence Interactions between Human and Rat Islet Amyloid Polypeptides. *Langmuir* **2014**, *30*, 5193–5201.
- (21) Wu, C.; Shea, J.-E. Structural Similarities and Differences between Amyloidogenic and Non-Amyloidogenic Islet Amyloid Polypeptide (Iapp) Sequences and Implications for the Dual Physiological and Pathological Activities of These Peptides. *PLoS Comput. Biol.* **2013**, *9*, e1003211.
- (22) Qi, R.; Luo, Y.; Ma, B.; Nussinov, R.; Wei, G. Conformational Distribution and Alpha-Helix to Beta-Sheet Transition of Human Amylin Fragment Dimer. *Biomacromolecules* **2014**, *15*, 122–31.
- (23) Xu, W.; Su, H.; Zhang, J. Z. H.; Mu, Y. Molecular Dynamics Simulation Study on the Molecular Structures of the Amylin Fibril Models. *J. Phys. Chem. B* **2012**, *116*, 13991–13999.
- (24) Li, Y.; Xu, W.; Mu, Y.; Zhang, J. Z. H. Acidic Ph Retards the Fibrillization of Human Islet Amyloid Polypeptide Due to Electrostatic Repulsion of Histidines. *J. Chem. Phys.* **2013**, *139*, 055102.
- (25) Laghaei, R.; Mousseau, N.; Wei, G. Structure and Thermodynamics of Amylin Dimer Studied by Hamiltonian-Temperature Replica Exchange Molecular Dynamics Simulations. *J. Phys. Chem. B* **2011**, *115*, 3146–3154.
- (26) Dupuis, N. F.; Wu, C.; Shea, J.-E.; Bowers, M. T. The Amyloid Formation Mechanism in Human Iapp: Dimers Have B-Strand Monomer-Monomer Interfaces. *J. Am. Chem. Soc.* **2011**, *133*, 7240–7243.

- (27) Bedrood, S.; Li, Y.; Isas, J. M.; Hegde, B. G.; Baxa, U.; Haworth, I. S.; Langen, R. Fibril Structure of Human Islet Amyloid Polypeptide. *J. Biol. Chem.* **2012**, *287*, 5235–5241.
- (28) Luca, S.; Yau, W.-M.; Leapman, R.; Tycko, R. Peptide Conformation and Supramolecular Organization in Amylin Fibrils: Constraints from Solid-State NMR. *Biochemistry (Moscow)* **2007**, *46*, 13505–13522.
- (29) Höppener, J. W. M.; Jacobs, H. M.; Wierup, N.; Sotthewes, G.; Sprong, M.; de Vos, P.; Berger, R.; Sundler, F.; Ahrén, B. Human Islet Amyloid Polypeptide Transgenic Mice: In Vivo and Ex Vivo Models for the Role of hIAPP in Type 2 Diabetes Mellitus. *Exp. Diabetes Res.* **2008**, *2008*, 1–8.
- (30) Goldsbury, C.; Goldie, K.; Pellaud, J.; Seelig, J.; Frey, P.; Muller, S. A.; Kistler, J.; Cooper, G. J. S.; Aeby, U. Amyloid Fibril Formation from Full-Length and Fragments of Amylin. *J. Struct. Biol.* **2000**, *130*, 352–362.
- (31) Wiltzius, J. J. W.; Sievers, S. A.; Sawaya, M. R.; Eisenberg, D. Atomic Structures of IAPP (Amylin) Fusions Suggest a Mechanism for Fibrillation and the Role of Insulin in the Process. *Protein Sci.* **2009**, *18*, 1521–1530.
- (32) Makin, S. O.; Serpell, L. C. Structural Characterisation of Islet Amyloid Polypeptide Fibrils. *J. Mol. Biol.* **2004**, *335*, 1279–1288.
- (33) Wang, L.; Middleton, C. T.; Singh, S.; Reddy, A. S.; Woys, A. M.; Strasfeld, D. B.; Marek, P.; Raleigh, D. P.; de Pablo, J. J.; Zanni, M. T.; et al. 2DIR Spectroscopy of Human Amylin Fibrils Reflects Stable B-Sheet Structure. *J. Am. Chem. Soc.* **2011**, *133*, 16062–16071.
- (34) Kayed, R.; Bernhagen, J.; Greenfield, N.; Sweimeh, K.; Brunner, H.; Voelter, W.; Kapurniotu, A. Conformational Transitions of Islet Amyloid Polypeptide (IAPP) in Amyloid Formation *in Vitro*. *J. Mol. Biol.* **1999**, *287*, 781–796.
- (35) Soong, R.; Brender, J. R.; Macdonald, P. M.; Ramamoorthy, A. Association of Highly Compact Type II Diabetes Related Islet Amyloid Polypeptide Intermediate Species at Physiological Temperature Revealed by Diffusion Nmr Spectroscopy. *J. Am. Chem. Soc.* **2009**, *131*, 7079–7085.
- (36) Berhanu, W. M.; Yaşar, F.; Hansmann, U. H. E. In Silico Cross Seeding of  $\text{A}\beta$  and Amylin Fibril-Like Oligomers. *ACS Chem. Neurosci.* **2013**, *4*, 1488–1500.
- (37) Bernhardt, N. A.; Berhanu, W. M.; Hansmann, U. H. E. Mutations and Seeding of Amylin Fibril-Like Oligomers. *J. Phys. Chem. B* **2013**, *117*, 16076–16085.
- (38) Nanga, R. P. R.; Brender, J. R.; Xu, J.; Veglia, G.; Ramamoorthy, A. Structures of Rat and Human Islet Amyloid Polypeptide IAPP1–19 in Micelles by NMR Spectroscopy. *Biochemistry (Moscow)* **2008**, *47*, 12689–12697.
- (39) Kale, L.; Skeel, R.; Bhandarkar, M.; Brunner, R.; Gursoy, A.; Krawetz, N.; Phillips, J.; Shinozaki, A.; Varadarajan, K.; Schulten, K. NAMD2: Greater Scalability for Parallel Molecular Dynamics. *J. Comput. Phys.* **1999**, *151*, 283–312.
- (40) Buck, M.; Bouquet-Bonnet, S.; Pastor, R. W.; MacKerell, A. D., Jr Importance of the Cmap Correction to the Charmm22 Protein Force Field: Dynamics of Hen Lysozyme. *Biophys. J.* **2006**, *90*, L36–L38.
- (41) Hess, B.; Kutzner, C.; van der Spoel, D.; Lindahl, E. Gromacs 4: Algorithms for Highly Efficient, Load-Balanced, and Scalable Molecular Simulation. *J. Chem. Theory Comput.* **2008**, *4*, 435–447.
- (42) Humphrey, W.; Dalke, A.; Schulten, K. Vmd - Visual Molecular Dynamics. *J. Mol. Graphics* **1996**, *14*, 33–38.
- (43) Reddy, A. S.; Wang, L.; Lin, Y. S.; Ling, Y.; Chopra, M.; Zanni, M. T.; Skinner, J. L.; De Pablo, J. J. Solution Structures of Rat Amylin Peptide: Simulation, Theory, and Experiment. *Biophys. J.* **2010**, *98*, 443–51.
- (44) Murphy, R. D.; Conlon, J.; Mansoor, T.; Luca, S.; Vaiana, S. M.; Buchete, N.-V. Conformational Dynamics of Human IAPP Monomers. *Biophys. Chem.* **2012**, *167*, 1–7.
- (45) Miller, Y.; Ma, B.; Nussinov, R. Synergistic Interactions between Repeats in Tau Protein and  $\text{A}\beta$  Amyloids May Be Responsible for Accelerated Aggregation Via Polymorphic States. *Biochemistry (Moscow)* **2011**, *50*, 5172–5181.
- (46) Guo, J.-P.; Arai, T.; Miklossy, J.; McGeer, P. L.  $\text{A}\beta$  and Tau Form Soluble Complexes That May Promote Self Aggregation of Both into the Insoluble Forms Observed in Alzheimer's Disease. *Proc. Natl. Acad. Sci. U.S.A.* **2006**, *103*, 1953–1958.
- (47) Seeliger, J.; Evers, F.; Jeworrek, C.; Kapoor, S.; Weise, K.; Andreetto, E.; Tolan, M.; Kapurniotu, A.; Winter, R. Cross-Amyloid Interaction of  $\text{A}\beta$  and IAPP at Lipid Membranes. *Angew. Chem., Int. Ed.* **2012**, *51*, 679–683.
- (48) Seeliger, J.; Weise, K.; Opitz, N.; Winter, R. The Effect of  $\text{A}\beta$  on IAPP Aggregation in the Presence of an Isolated B-Cell Membrane. *J. Mol. Biol.* **2012**, *421*, 348–363.
- (49) Giasson, B. I.; Forman, M. S.; Higuchi, M.; Golbe, L. I.; Graves, C. L.; Kotzbauer, P. T.; Trojanowski, J. Q.; Lee, V. M.-Y. Initiation and Synergistic Fibrillization of Tau and Alpha-Synuclein. *Science* **2003**, *300*, 636–640.
- (50) Yu, X.; Wang, J.; Yang, J.-C.; Wang, Q.; Cheng, S. Z. D.; Nussinov, R.; Zheng, J. Atomic-Scale Simulations Confirm That Soluble [Beta]-Sheet-Rich Peptide Self-Assemblies Provide Amyloid Mimics Presenting Similar Conformational Properties. *Biophys. J.* **2010**, *98*, 27–36.
- (51) Siddiqua, A.; Luo, Y.; Meyer, V.; Swanson, M. A.; Yu, X.; Wei, G.; Zheng, J.; Eaton, G. R.; Ma, B.; Nussinov, R.; et al. Conformational Basis for Asymmetric Seeding Barrier in Filaments of Three- and Four-Repeat Tau. *J. Am. Chem. Soc.* **2012**, *134*, 10271–10278.
- (52) Meyer, V.; Dinkel, P. D.; Luo, Y.; Yu, X.; Wei, G.; Zheng, J.; Eaton, G. R.; Ma, B.; Nussinov, R.; Eaton, S. S.; et al. Single Mutations in Tau Modulate the Populations of Fibril Conformers through Seed Selection. *Angew. Chem., Int. Ed.* **2014**, *53*, 1590–1593.
- (53) Jiang, P.; Wei, L.; Pervushin, K.; Mu, Y. pH-Dependent Interactions of Human Islet Amyloid Polypeptide Segments with Insulin Studied by Replica Exchange Molecular Dynamics Simulations. *J. Phys. Chem. B* **2010**, *114*, 10176–10183.
- (54) Dupuis, N. F.; Wu, C.; Shea, J.-E.; Bowers, M. T. Human Islet Amyloid Polypeptide Monomers Form Ordered B-Hairpins: A Possible Direct Amyloidogenic Precursor. *J. Am. Chem. Soc.* **2009**, *131*, 18283–18292.
- (55) Zhang, Y.; Luo, Y.; Deng, Y.; Mu, Y.; Wei, G. Lipid Interaction and Membrane Perturbation of Human Islet Amyloid Polypeptide Monomer and Dimer by Molecular Dynamics Simulations. *PLoS One* **2012**, *7*, e38191.
- (56) Andrews, M. N.; Winter, R. Comparing the Structural Properties of Human and Rat Islet Amyloid Polypeptide by MD Computer Simulations. *Biophys. Chem.* **2011**, *156*, 43–50.
- (57) Kajava, A. V.; Aeby, U.; Steven, A. C. The Parallel Superpleated Beta-Structure as a Model for Amyloid Fibrils of Human Amylin. *J. Mol. Biol.* **2005**, *348*, 247–252.
- (58) Wiltzius, J. J. W.; Sievers, S. A.; Sawaya, M. R.; Cascio, D.; Popov, D.; Riek, C.; Eisenberg, D. Atomic Structure of the Cross-Beta Spine of Islet Amyloid Polypeptide (Amylin). *Protein Sci.* **2008**, *17*, 1467–1474.